

# Multi-Physical Simulation of Aerostatic Bearings

L. Lentini<sup>1</sup>, F. Colombo<sup>1</sup>, A. Trivella<sup>1</sup>, T. Raparelli<sup>1</sup>, V. Viktorov<sup>1</sup>

1. Department of Mechanical and Aerospace Engineering, Politecnico di Torino, Turin, Italy

## 1. Introduction

Because of their almost zero friction and wear, aerostatic pads are commonly used in applications where high precision of positioning is required, e.g., machine tools, measuring machines and system for power board testing [1].

However, in many such applications, the reliability of numerical models and the performance of aerostatic pads are strictly related to their manufacturing accuracy and their mechanical properties. In fact, it has been experienced that the performance of these bearings can be significantly influenced by manufacturing errors and deformations [2].

This paper presents a numerical and experimental study that investigates the influence of these phenomena on the reliability of aerostatic pad models.

## 2. Experimental Set-up

Figure 1 shows a photograph of the aerostatic pad that has been considered in this study.

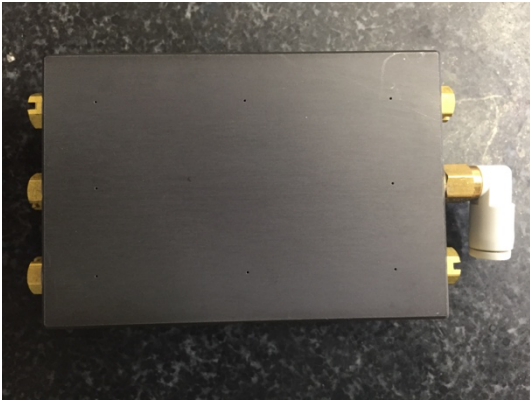


Figure 1. Photograph of the aerostatic pad under investigation.

As can be seen, the pad presents eight supply holes with a diameter  $d_s=0.2$  mm that are distributed on a supply rectangle of size 55 mm x 30 mm. The pad was tested in static conditions in the presence of a gauge supply pressures equal 0.5 MPa. Figure 2 shows the test bench that has been used to obtain the load capacity and air consumption curves of the pad. As can be seen the static test bench consists of a metal basement, a sensors carrier, a pneumatic cylinder, a load cell and a loading tip. Once the pad was located on the basement, varying the supply pressure of the cylinder ( $P_{sCylinder}$ ) made it possible to modify the external load applied to the pad. This load was transmitted through a mechanical chain composed of the load cell, a connection element and the loading tip. Four capacitive sensors mounted on a sensor carrier were used to measure the pad displacement. The air gap height was evaluated as the difference between the pad positions with and without supply air. Additionally, a flowmeter, was used to measure the air consumption of the pad.

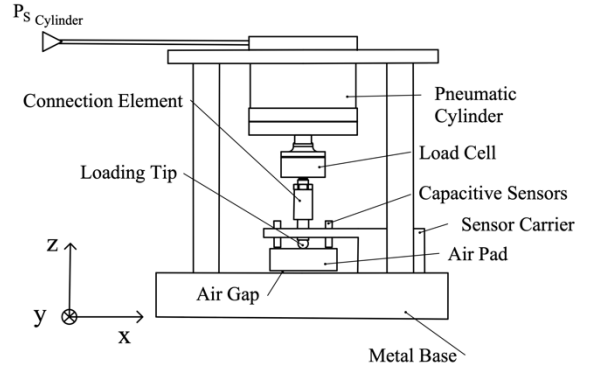


Figure 2. Scheme of the static test bench.

## 3. Numerical model

The static performance of the pad was simulated via COMSOL Multiphysics. The air pad modelling consists of two main parts. The first is defining a suitable formulation to model the air flow supplied through the pad restrictors. This theoretical flow rate was computed using the formulation proposed in [3]:

$$G_{hole} = c_d \frac{\overbrace{\pi d_s^2}^A}{4} \frac{p_s}{\sqrt{RT_s}} \sqrt{\frac{2k}{k-1} \left( \bar{p}^{\frac{2}{k}} - \bar{p}^{\frac{k+1}{k}} \right)} \quad (1)$$

$$\bar{p} = \begin{cases} \frac{p_c}{p_s}, & \frac{p_c}{p_s} > b = 0.5283 \\ \left( \frac{2}{k+1} \right)^{\frac{k}{k-1}}, & \frac{p_c}{p_s} \leq b = 0.528 \end{cases}$$

where,  $A$  is the cross-section of the supply restrictors,  $p_s$  and  $T_s$  are the supply pressure and supply temperature of the pad,  $k$  and  $R$  are the ratio of specific heats and the gas constant of the lubricant.  $c_d$  is a discharge coefficient that depends on the Reynolds' number ( $Re$ ) and the ratio between the air gap and orifice dimensions ( $h/d_s$ ):

$$c_d = 0.95 \left( 1 - e^{-8.2 \frac{h}{d_s}} \right) (1 - 0.3e^{-0.001 Re})$$

where,

$$Re = \frac{4G}{\pi \mu d_s}$$

and  $\mu$  is the air viscosity.

The second part of the modelling of the thin film flow domain. Being a compressible flow, this domain is described using the stationary isothermal (or modified) Reynolds' equation:

$$\frac{\partial}{\partial x} \left( \frac{ph^3}{12\mu} \frac{\partial p}{\partial x} \right) + \frac{\partial}{\partial y} \left( \frac{ph^3}{12\mu} \frac{\partial p}{\partial y} \right) = 0 \quad (2a)$$

that in COMSOL is equivalently expressed as:

$$\nabla \cdot (hp\mathbf{v}_{ave}) = 0 \quad (2b)$$

where,  $p$  is the local<sup>1</sup> air gap pressure,  $h$  is the local air gap height and  $\mathbf{v}_{ave}$  is the local average velocity of the fluid:

$$\mathbf{v}_{ave} = v_{ave,x}\hat{\mathbf{i}} + v_{ave,y}\hat{\mathbf{j}} \quad (3)$$

whose scalar components correspond to the air flow rate per unit depth ( $q_x, q_y$ ) divided by the local air gap height  $h$ :

$$v_{ave,x} = \frac{1}{h} \int_0^h u(z) dz = \frac{q_x}{h} \quad (4a)$$

$$v_{ave,y} = \frac{1}{h} \int_0^h v(z) dz = \frac{q_y}{h} \quad (4b)$$

The boundary conditions prescribed for the thin film flow model where ambient pressure at the edge of the pad and the unknown pressure  $p_c$  in the correspondence of the restrictor outlet.

These two parts of the model have to be related considering that the pressure downstream the air pad restrictors ( $p_c$ ) corresponds to the inlet pressure supplied to the air gap. This can be done considering one additional (global equation) continuity equation in the correspondence of each supply hole:

$$G_{hole} - G_{gap} = 0 \quad (5)$$

$$G_{gap} = \oint_{\Gamma} (\rho h \mathbf{v}_{ave}) \cdot \hat{\mathbf{n}} dl \quad (6)$$

where,  $\Gamma$  stands for the boundary through which the flow enters, and  $\hat{\mathbf{n}}$  is the unit normal to the boundary.

These equations have to be solved for  $p_c$  by considering a scaling factor of  $10^{10}$  due to the different order of magnitude existing between the values of the air mass flow rates  $G_{hole/gap}$  and the searched values of pressures  $p_c$ . The initial values adopted to solve these nonlinear equations were taken equal to  $0.999 p_s$ .

In order to solve the fluid structure interaction problem, it was necessary to divide the simulation in two successive steps:

1. Solving the flow problem ( $p_c$ )
2. Using the results of the flow problem as initial values for the model that consider the FSI

The only differences between the model describing the flow and the FSI problems are that considering the solid mechanics needs to define additional conditions. In particular, the air gap pressure was applied as boundary load and the structure of the pad was constrained on the line where the external load is applied.

## 4. Results and Discussions

The main goal of the analysis was to compare the discrepancy between model and experimental results under the following assumptions:

- Flat rigid pad
- Flat rigid pad with a tilting about the mid-point
- Concave rigid pad
- Flat deformable pad
- Flat deformable pad with a tilting about the mid-point
- Concave deformable pad

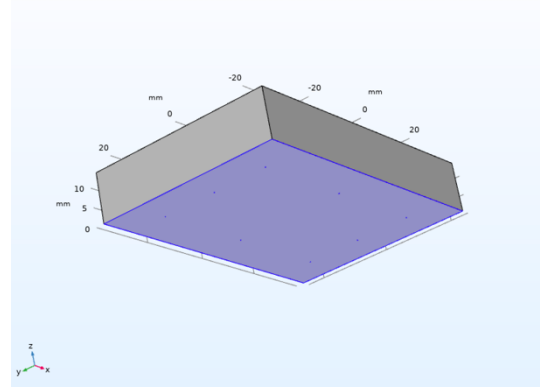


Figure 3. Boundary load applied to the pad structure.

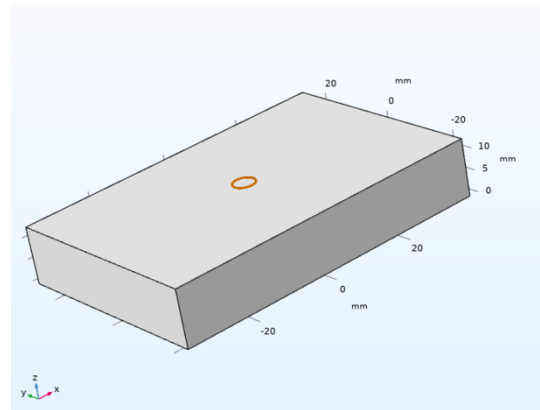


Figure 4. Application of the fixed constraint to the pad structure.

For the sake of brevity, the comparison of the numerical load capacity and air consumption of the pad was performed considering only a supply gauge pressure of 0.5 MPa. This choice was dictated by the fact that this value is one of the most used in aerostatic bearing applications.

<sup>1</sup> Is the value assumed at each node of the calculation grid.

Regarding the effect of the tilting, it was found that, theoretically, the tilting has no effect<sup>2</sup>. Figure 5 shows the comparison between experimental and numerical results obtained considering a rigid and deformable bearing in the presence and the absence of tilting.

In fact, the numerical curves obtained with a rigid and a deformable pad in the presence and absence of tilting exhibit a perfect match (see Figures 5 and 6). This can be easily explained by considering the air gap pressure profile. As can be seen in Figure 7, the theoretical tilting modifies only locally the pressure distribution maintaining unaltered the global features of the pad. Conversely, it is interesting to see that considering the pad deformation makes it possible to significantly reduce the discrepancies between experimental and numerical results. This is due to the fact that the air gap pressure deforms the bearing land thus reducing the bearing performance [4]. This fact can be easily figured out by considering Figure 8 where it is possible to see that magnitude of the bearing deflection is not negligible especially in the presence of low air gap heights.

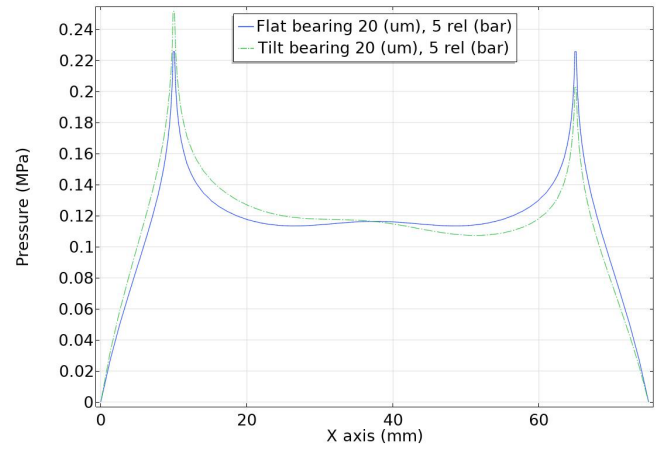


**Figure 7.** Comparison between the pressure profile of the rigid flat bearing obtained in the presence and the absence of tilting.

Gap(1)=5E-6 m Surface: Displacement field, Z component ( $\mu\text{m}$ )

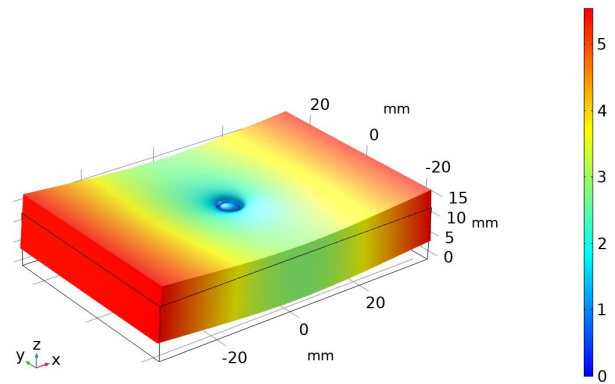


**Figure 8.** Deformed shape of the pad in the presence of an air gap height of  $5 \mu\text{m}$ .

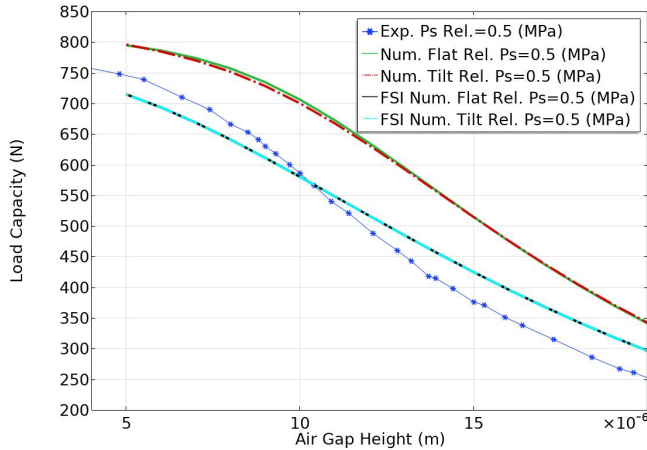


**Figure 5.** Load capacity curves considering a rigid and deformable bearing in the presence and the absence of tilting.

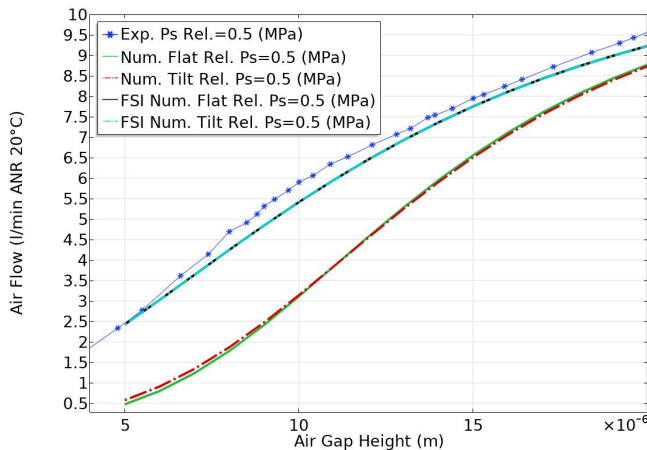


**Figure 6.** Air consumption curves considering a rigid and deformable bearing in the presence and the absence of tilting.

The higher performance of concave pads was confirmed by comparing the characteristic curves of the pad obtained in the presence and the absence of concavity.

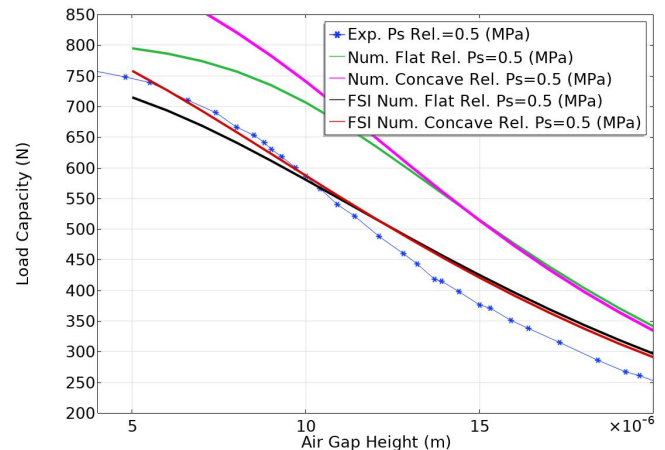


**Figure 9.** Load capacity curves considering a rigid and deformable bearing in the presence and the absence of concavity.

<sup>2</sup> It is fundamental to clarify that the numerical tilting can be different from the experimental one depending on how t

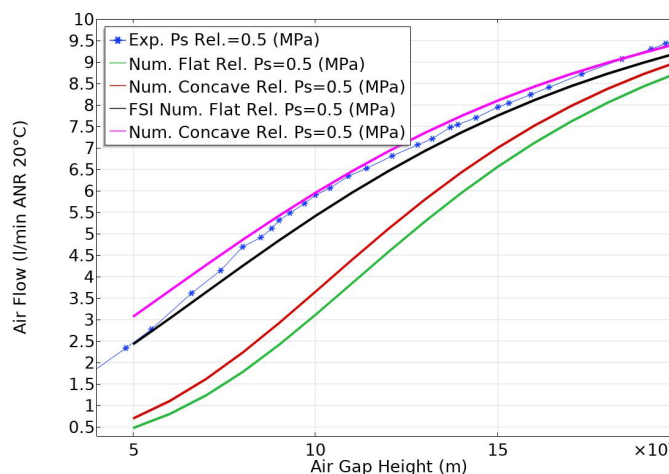


**Figure 10.** Air consumption curves considering a rigid and deformable bearing in the presence and the absence of concavity.

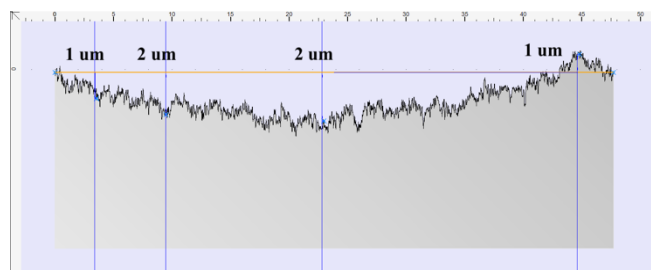


**Figure 11.** Experimental profile of the pad.

Moreover, the better results obtained through the concave deformable model of the pad was experimentally explained by measuring the real profile of the pad. In fact, as it can be seen from Figure 11, it was found that the pad surface exhibit a concavity with a maximum depth of  $2\ \mu\text{m}$ .

## 5. Conclusions

This paper has presented a numerical and experimental investigation on some of the main parameter that can compromise the accuracy aerostatic pad numerical models: shape of the bearing land (concavity/convexity), tilting and deformations. It was found that the theoretical tilting has no effect on the pad performance.

Conversely, the shape of the bearing land and the deflection exhibited by the pad significantly compromise the accuracy of numerical predictions.

## 6. References

1. L. Lentini, M. Moradi, and F. Colombo, *Tribology in Industry* **40**, 165 (2018).
2. Y. B. P. Kwan and J. B. Post, *Tribology International* **33**, 581 (2000).
3. G. Belforte, T. Raparelli, V. Viktorov, and A. Trivella, *Tribology International* **40**, 512 (2007).
4. F. Colombo, L. Lentini, T. Raparelli, V. Viktorov, and A. Trivella, in *Advances in Mechanism and Machine Science*, edited by T. Uhl (Springer International Publishing, 2019), pp. 3919–3928.